SLAC-PUB-12128
September 2006

Coherent instabilities of ILC damping rings. [1]

S. Heifets , G. Stupakov, and K. Bane,
Stanford Linear Accelerator Center, Stanford University, Stanford, CA 94309, USA

1 Parameters

The paper presents the first attempt to estimates the ILC damping ring impedance and compare thresholds of the classical instabilities for several designs initially proposed for the DR. The work was carried out in the spring of 2006. Since then the choice of the DR is narrowed. Nevertheless, the analysis described below may be useful for the next iterations of the beam stability.

We use parameters for the damping rings vacuum chamber from A. Wolsky's paper [1]. They are summarized in the following Table I1 where $\tau_{l,y}$ are the SR longitudinal and vertical damping times, respectively.

Ring	PPA	OTW	OCS	BRU	MCH	DAS	TESLA
C (m)	2824	3223	6114	6333	15935	17014	17000
$I_{dc,beam}$, (mA)	959	839	443	426	170	159	159
$I_{dc,bunch}$, (mA)	0.408	0.326	0.157	0.152	0.0603	0.0565	0.0565
I_{peak}, (A)	76.7	70.0	63.9	42.6	42.6	63.9	63.9
V_{rf},(MeV/ring)	17.76	21.78	19.27	23.16	53.7	48.17	50.
Q_y	47.680	24.157	40.800	66.413	76.413	83.65	41.18
Q_s	0.0269	0.0418	0.0394	0.120	0.150	0.0668	0.07
$\alpha * 10^3$	0.283	0.362	0.159	1.19	0.409	0.114	0.122
σ,(mm)	6.	6.	6	9.	9.	6.	6.
$\delta_0\, 10^3$	1.27	1.36	1.29	0.973	1.30	1.3	1.29
$\langle\beta_y\rangle$, (m)	12.5	63.8	31.0	55.4	108.0	106.0	121.0
τ_l, (ms)	10.0	6.07	11.1	12.8	13.4	13.5	13.9
τ_y, (ms)	20.	12.1	22.2	25.5	26.9	27.	27.9
Quads/ring	768	240	760	850	1038	808	946
L Arcs, (m)	2709.0	1002.0	5846.0	3634.0	3634.0	3240.0	2229.0
L Wigglers, (m)	115.0	202.0	268.0	540.0	540.0	560.0	529.0
L Straights, (m)	0.0	2019.0	0.0	2159.0	11761.0	13214.0	14242.0

Table 1: Parameters of the rings.

[1] Work supported by Department of Energy contract DE-AC02-76SF00515

The transverse dimensions (half gap or radius) of the beam pipe are assumed to be the same for all machines: $b = 22/8/49$ mm for arcs, wigglers, and straight sections, respectively. Aluminum beam pipe is implied everywhere with the resistivity $\rho = 0.17\,10^{-7}\ Ohm\,m$.

The number of quads is used to estimate the number of optical cells which, in turn, used to scale impedance of the vacuum components in the ring.

2 Impedance models

We model the total impedances and wakes of a ring as the sum of the contributions of the HOMs in the rf cavities, resistive wall (RW), and vacuum components in the ring.

2.1 Higher order modes in super-conducting cavities

Design of some rings specifies the number of cavities. In this study, for comparison, we rather assume the same type of RF cavities for all rings and, defining the number of rf cavities n_{cav}, we use the voltage per ring (from Table. I) and 2 MV voltage per cavity. (For comparison, voltage per cavity for CESR is 1.8 MeV; for KEKB - 1.6/2.0, and for LHC 2.0 MeV.) Reported accelerating gradient up to 20-25 MeV/m at 4.5 K may give 4-5 MeV for a gap $g = 20$ cm. TESLA DR specifies the gradient of 15 MV/m and the active length 0.3 m which gives 4.5 MV voltage per cavity with the total number of cavities equal to 12., so that the calculated number of cavities (see Table 2) may not agree with the design number (e.g., the TESLA design [2] specifies 12 cavities rather than 25 in the table).

Ring	PPA	OTW	BRU	OCS	MCH	DAS	TESLA
Number of cavities	8	10	9	11	26	24	25

Table 2: Number of superconducting RF cavities n_{cav} in the rings.

We assume that the superconductive (SC) rf cavities are one cell cavities in a cryomodule although in reality SC cavities can be arranged in pairs per one cryomodule. The impedance relevant for the beam stability of the cryomodule is defined by the impedances of the HOMs of the SC cavity (excluding the fundamental mode), ferrite loading and tapers connecting the SC cavity with the beam pipe. We do not consider here questions related to the beam loading. Parameters of the HOMs given in Table 3, 4 and which were used in calculations are borrowed from the KEK Design Report [3]. Note that R/Q is defined as $R/Q = V^2/P$, therefore the loss factor of a mode $\kappa = (\omega/4)(R/Q)$.

The narrow-band impedance is given as the sum of contributions of all modes listed in the Tables 3 and 4,

$$Z_l(\omega_) = n_{cav} \sum \frac{(R/Q)_l Q_L}{1 - iQ_L(\omega/\omega_l - \omega_l/\omega)},$$
$$Z_t(\omega_) = n_{cav} \sum \frac{(\omega_t/\omega)\,(R/Q)_t\,Q_t}{1 - iQ_t(\omega/\omega_t - \omega_t/\omega)}. \quad (1)$$

f_l, (MHz)	783.0	834.0	1018.0	1027.0	1065.0	1076.0	1134.0
$(R/Q)_l$, (Ohm)	0.12	0.34	6.6	6.4	1.6	3.2	1.7
Loaded Q_L,	132	72	106	95	76	65	54

Table 3: Longitudinal HOMs of KEK SC RF cavity.

f_t, (MHz)	609.0	648.0	688.0	705.0	825.0	888.0
$(R/Q)_t$, (Ohm/m)	1.9	40.2	170.4	227.3	6.16	3.52
Q_t,	92	120	145	94	60	97

Table 4: Transverse HOMs of KEK SC RF cavities.

The total loss factor of fundamental mode is 0.15 V/pC and of the HOMs is only 0.065 V/pC. The total loss factor of the KEK cryomodule, $\kappa_l = 2.3$ V/pC, is dominated by the contribution of the tapers and loads and is taken into account below together with the rest of the vacuum components.

2.2 Resistive wall impedance

The vertical resistive wall wake field

$$W_y(s) = \frac{A_y}{\sqrt{z}}, \quad A_y = \frac{4C}{\zeta}\sqrt{\frac{\rho}{\pi Z_0}}\,\langle\frac{1}{b^3}\rangle, \quad (2)$$

where C is ring circumference, $Z_0 = 120\pi$ Ohm, ρ is the wall resistivity, and $\zeta = 111$ is conversion factor, 111 $1/m$ is equal to one V/pC. The averaged factor $\langle 1/b^3\rangle$ is calculated from the apertures of the arcs, wigglers, and straight sections weighted proportional to the length of these components.

The RW loss factor

$$\kappa_l = \frac{\Gamma[3/4]}{\pi\sigma_l b_{aver}}\,(\frac{\rho_{Al}}{2Z0\sigma_l})^{1/2}\,C \quad (3)$$

is

$$\frac{\kappa_l}{V/pC} = \{6.10561, 4.97286, 13.2859, 6.68852, 11.4246, 21.6208, 20.3398\}. \quad (4)$$

2.3 Broadband impedance

The impedance of the numerous vacuum components is mostly inductive. It can be defined by two parameters: inductance of the ring L and the total loss factor of these components κ_L,

$$Z_l(\omega) = -i\frac{Z_)}{4\pi}\,\frac{\omega L/c}{(1-i\omega a/c)^{3/2}}, \tag{5}$$

where parameter a has to be chosen to give the loss factor κ_L at the bunch length σ_l,

$$\kappa_L(\sigma_l) = \int Z(\omega) e^{-(\omega\sigma_l/c)^2}\,\frac{d\omega}{2\pi}. \tag{6}$$

$Z(\omega)$ is the pure inductive impedance at low frequencies but rolls off as $1/\sqrt{\omega}$ at large frequencies according to the diffraction model.

Inductance L is obtained from the inductance $L_{PEP} = 100$ nH estimated for the vacuum components of PEP-II LER by scaling proportional to the number N_{quads} of quads in the ring and with the beam pipe radius,

$$L = L_{PEP}\,(\frac{N_{quads}}{N_{PEP}})\,(\frac{b_{PEP}}{b})^2 + n_{cav}L_{SC}. \tag{7}$$

For PEP-II, $N_{PEP} = 292$ and $b_{PEP} = 3.15$ cm. The last term takes into account inductance of the cryomodule tapers. The inductance of a taper $L_{SC} = 0.45$ nH is estimated using Yokoya's formula $L = l\alpha^2$, the taper angle $\alpha = 10^o$ and the taper length $l = 15$ cm.

The loss factor κ_l is taken as the sum of the PEP-II loss factor κ_{PEP} and the loss factors of the SC cryomodules κ_{SCM},

$$\kappa = \kappa_{PEP}(\frac{N_{quads}}{N_{PEP}})(\frac{\sigma_{PEP}}{\sigma})^2 + n_{cav}\kappa_{SCM}. \tag{8}$$

The PEP-II loss factor (without IR) has been estimated as $\kappa_{PEP} = 2.5$ V/pC at $\sigma_{PEP} = 10$ mm. It is scaled here with the number of quads and with the bunch length as $(1/\sigma)^2$, which is the measured in PEP-II σ-dependence typical for a tapers. The loss factor of a cryomodule κ_{SCM} is obtained from $\kappa_{SCM} = 0.5$ V/pC at $\sigma_l = 10$ mm by scaling proportional to $1/\sigma$. Such a dependence approximately reproduces the experimental σ dependence of the KEK SC module loss factor.

The loss factor κ defines the roll-off parameter a of the inductive impedance. Results are summarized in the Table 5.

An example of the longitudinal wake of the inductive components PPA machine convoluted with 1 mm Gaussian bunch is shown in Fig. 1.

The transverse impedance is calculated as the sum of the HOMs of the SC rf cavities, transverse RW impedance, and the transverse impedance Z_t of the vacuum components scaled from the longitudinal impedance Z_l, $Z_t(\omega) = (2R/b^2)Z_l(n)/n$, where $n = (\omega_0/\omega)$. Example of the transverse narrow-band

L, (nH)	340.6	118.5	276.8	281.7	290.2	212.7	216.7
a, (cm)	0.07	0.11	0.09	0.17	0.35	0.22	0.27
κ_{SC}, (V/pC)	5.8	7.2	6.5	4.9	11.6	17.4	18.1
κ, (V/pC)	24.1	12.9	24.6	13.9	22.6	36.6	40.6

Table 5: Estimate of the inductance L, roll-off parameter a, broad-band loss factor κ_{SC} of cryomodules in the ring, and the total loss factor κ of vacuum components.

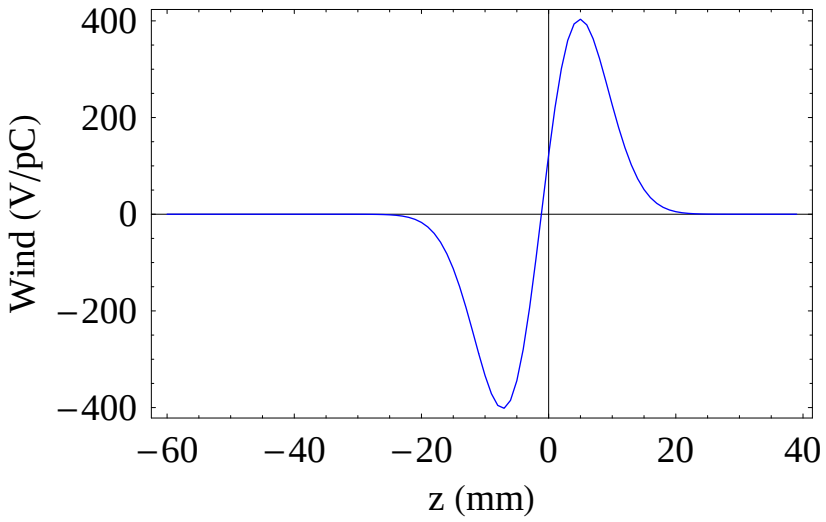

Figure 1: Longitudinal wake of the vacuum components for PPA convoluted with 1mm Gaussian bunch.

impedance (in the range of frequencies corresponding to HOMs) is shown in Fig.2.

The magnitude of the overall impedance of a machine can be illustrated by the parameter $|Z(n)/n|$ defined as

$$|\frac{Z}{n}| = \frac{\sigma}{R\sqrt{\pi}} \sum_{n=-\infty}^{\infty} \frac{Z[n\omega_0]}{n} e^{-n^2(\frac{\sigma\omega_0}{c})^2}. \tag{9}$$

Calculations give

$$|\frac{Z}{n}| = \{246, 94, 210, 214, 155, 116, 107\} \text{ mOhm}. \tag{10}$$

Our estimate is based on assumption that the number of vacuum components is scaled proportional to the number of quadrupoles in the ring which is roughly

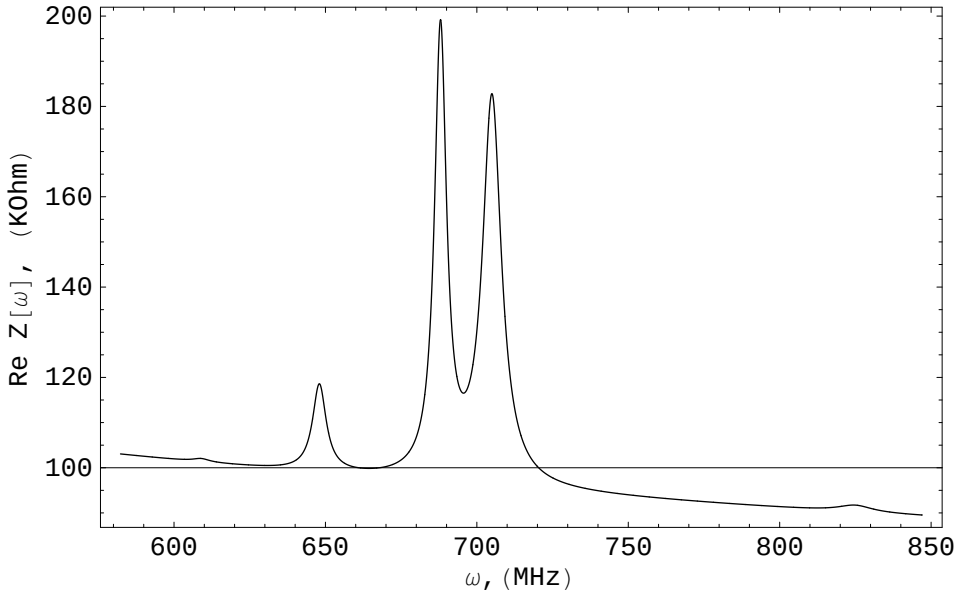

Figure 2: Narrow-band total transverse impedance wake for PPA.

proportional to the number of optical cells in the ring. That is, probably, the best what we can assume now. However, such scaling may be wrong. For example, the very long cells of straight sections can have few quads, but the number of vacuum pumps can be large to avoid the pressure instability.

3 Multibunch instabilities

3.1 Multibunch transverse instability

The growth rate of the l-th coupled-bunch(CB) mode of the transverse multi-bunch instability is given by imaginary part of the coherent frequency shift [4]:

$$\Delta\omega_y(l) = -i\frac{I_{beam}\omega_0}{4\pi(E/e)}\sum_{p=-\infty}^{\infty}\beta_y Z_y[\omega_\beta + (pM+l)\omega_0] \tag{11}$$

where $Z_y(\omega)$ is the transverse impedance, $I_{beam} = eN_eMf_0$ is the average beam current, $f_0 = \omega_0/(2\pi)$ is revolution frequency, E is the beam energy, and M is the number of bunches in the ring. The formula assumes a uniform distribution of bunches in the ring and assumes a point-like bunches with the charge equal to N_e.

The summation can be carried out analytically, if one uses wake-fields instead of impedances.

The main contribution to the growth rate of the CB transverse instability is given by the RW impedance. For the resistive wall the transverse wake decays with distance as $w_t = Az^{-1/2}$, where

$$A = \frac{4C}{b^3}\sqrt{\frac{\rho}{\pi Z_0}}. \tag{12}$$

The approximate value of the growth rate of the instability

$$\Gamma = \mathrm{Im}\,\Delta\omega(l) = \frac{AI_{beam}\beta_y}{4(E/e)\sqrt{2\pi R(1-\{\nu_y\})}}, \tag{13}$$

where $\{\nu_y\}$ means the fractional part of the tune. The growth rate can be reduced choosing tune below half-integer.

The growth rate Γ for the instability and the factor A is given in Table 6.

Ring	PPA	OTW	OCS	BRU	MCH	DAS	TESLA
A, V/(pC$\cdot\sqrt{\mathrm{m}}$)	80.87	85.40	181.1	238.8	252.6	255.0	230.2
Γ_g $(1/ms)$	1.38	0.80	3.28	1.75	0.54	0.49	0.42
Γ_g, turns	77.0	116.	14.9	27.0	34.6	35.7	42.4

Table 6: The growth time for the multi-bunch transverse instability due to resistive wall impedance.

The growth rate is substantially depend on the beam pipe aperture. Results shown in Table 6 correspond to the set $b_{Arcs}/b_{wigg}/b_{str} = 22/8/49$ mm and requires the transverse feedback system (TFB) which is stronger than the available state-of-the-art TFB which can handle the growth time not less than 15 turns. Increasing apertures to the larger values (mostly in the wigglers) $b_{Arcs}/b_{wigg}/b_{str} = 25/16/49$ mm makes the growth time much more acceptable. The growth time in number of turns in this case is

$$\tau = \{113., 164., 17.8, 55.1, 50.0, 49.6, 63.6\}\,\text{turns}. \tag{14}$$

The tune shift $\Delta\nu_y \simeq (\Gamma/\omega_0)$ caused by the RW impedance is equal to the growth rate Γ. Generally speaking, it can vary along the bunch train and distort optics for bunches in the tail of the train. However, effect is very small,

$$\Delta\nu_y = 10^{-3} * \{2.1,\ 1.36,\ 10.6,\ 5.9,\ 4.6,\ 4.46,\ 3.76\}. \tag{15}$$

In the calculations we implied that the skin depth for the frequencies equal to $\{\nu_y\}\omega_0$ is small compared with the thickness of the vacuum chamber.

The growth rate calculated with the total transverse impedance differs very little from the result obtained with the pure RW, see Fig.3

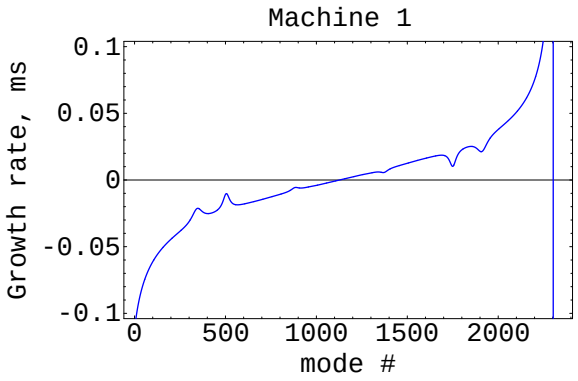

Figure 3: Transverse CB instability with the total impedance for PPA. The pure RW impedance would give a smooth curve with the same fastest growth rate.

3.2 Multibunch longitudinal instability due to HOMs

Contrary to the RW instability, the coupled-bunch longitudinal instability does not look dangerous. The coherent tune shift of the l-th rigid longitudinal coupled-bunch oscillations is [4]

$$\Delta\Omega_l = i\frac{\alpha I_{beam}\omega_0}{4\pi(E/e)Q_s}\sum_{p=-\infty}^{\infty} p_{eff}\, Z_l[p_{eff}]\, e^{-(p_{eff})^2(2\pi\sigma_l/C)^2}, \qquad (16)$$

where $p_{eff} = pn_b + l + Q_s$. The instability of the l-th mode corresponds to the positive values of the growth rate $\Gamma_l = Im[\Delta\Omega_l]$.

An example of the growth rate for all modes in the PPA machine is shown in Fig. 4. The maximum growth rate Γ for several machines is given in the Table 7. In all cases, the threshold current I_{th} defined by the SR damping time is higher than the nominal beam current at least by an order of magnitude.

Ring	PPA	OTW	OCS	BRU	MCH	DAS	TESLA
Γ, $(1/ms)$	0.0034	0.00297	0.000767	0.0025			
I_{beam}, (A)	27.73	46.51	52.0	13.3			

Table 7: The growth rate Γ of a strongest mode and the threshold current I_{th} for the CB longitudinal instability.

It is worth noting that the typical Q factor for the HOMs in SC cavities using ferrite HOM absorbers is of the order of 100. For the frequencies of HOMs in the range from 1 to 3 GHz this means that the width of the resonance of each mode $\Delta f_{\rm res}$ is of the order of 10 to 30 MHz. In the sum of Eq. (11) the summation over the frequency goes with the step equal to $M\omega_0$. For the typical number

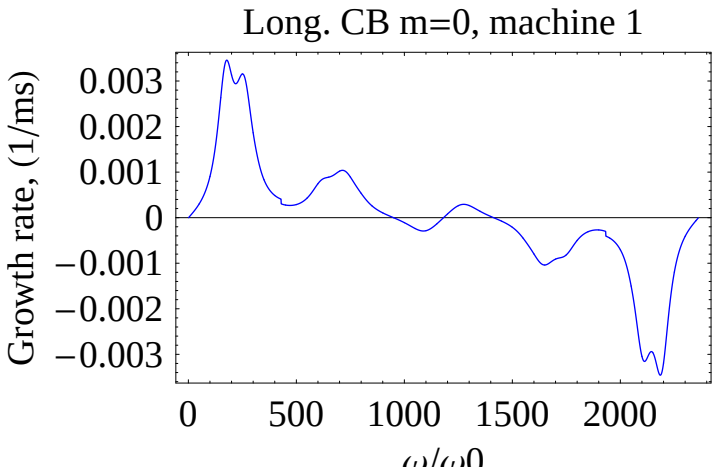

Figure 4: Longitudinal CB instability

of bunches in the ILC damping ring $M \sim 3000$ and the revolution frequencies from $2\pi \times 100$ kHZ for a 3-km ring to $2\pi \times 18$ kHZ for a 17-km ring, we find that $\Delta f_{\rm res} \gtrsim M\omega_0/2\pi$, which means that for each oscillation mode l the dominant contribution comes from only one term in the sum.

The transient beam loading in the SC cavities due to gaps in the bunch train is known to cause rf phase variation of the individual bunches. Effect, however, should be small due to high Q-factor of the SC cavities.

3.3 Bunch lengthening

We study the bunch lengthening solving the Haissinski equation by the Newton's method as it was suggested by R. Warnock. Results of calculations show that the bunch length σ changes linearly with current and is given below in terms of $d\sigma/dI_{bunch}$,

$$\frac{d\sigma}{dI_{bunch}} = \{0.0250,\ 0.0053,\ 0.033,\ 0.0098,\ 0.0060,\ 0.017,\ 0.011\}\,(\frac{\rm mm}{\rm mA}). \quad (17)$$

3.4 Microwave instability

To evaluate the microwave instability we use Boussard-Schnell criterion

$$\frac{Z}{n} = Z_0\sqrt{\frac{\pi}{2}}\frac{\alpha\gamma\sigma_\delta^2\sigma_z}{N_p r_e}\,. \quad (18)$$

This gives the values Z/n shown in Table 8 where for comparison we also give the estimated Z/n obtained above.

Ring	PPA	OTW	OCS	BRU	MCH	DAS	TESLA
$(Z/n)_t$, mOhm	187	300	621	132	509	95	100
$(Z/n)_e$, mOhm	246	94	210	214	155	116	107
Threshold $I_{thbunch}$, mA	0.31	1.04	0.44	0.098	0.20	0.046	0.052
Nominal $I_{nombunch}$, mA	0.41	0.32	0.16	0.15	0.06	0.056	0.056

Table 8: Estimates for the microwave instability. The table gives the tolerable $(Z/n)_t$ and estimated $(Z/n)_e$ values of the impedance Z/n as well as the threshold I_{th} and the nominal I_{nom} bunch currents.

Taken literary, the result means that PPA, BRU rings may have the microwave instability, while DAS and TESLA are close to the threshold. In a sense, that contradicts results for bunch lengthening which is small for all machines. To check the situation, we used the Oide's code for microwave instability. The result for PPA machine shown in Fig. 5 predicts the threshold of the microwave instability around $N_e = 2.\,10^{10}$ particles per bunch. The independent tracking code with 10^5 macroparticles, however, shows that the bunch is stable even at $N_e = 5\,10^{10}$. We are planing to make more elaborate calculations using the Fokker-Plank solver and tracking when more detail impedance model will be available.

3.5 Transverse mode coupling instability

We use the following criterion for the threshold peak current of the instability

$$I_{\rm peak} <= \frac{16\sqrt{\pi}}{3}\frac{(E/e)\nu_s\sigma_z}{{\rm Im}\,(Z_\perp\beta_\perp)\,R}\,. \tag{19}$$

The peak current of the machines are listed in Table I. The tolerable values of the product ${\rm Im}\,Z_\perp\beta_\perp$, are given in Table 9.

Ring	PPA	OTW	BRU	OCS	MCH	DAS	TESLA
${\rm Im}\,Z_\perp\beta_\perp$, kOhm	0.22	0.33	0.16	0.89	0.60	0.11	0.12

Table 9: The tolerable values of ${\rm Im}\,Z_\perp\beta_\perp$ given by the mode coupling instability.

We studied the transverse mode coupling (MC) instability in more detailes following Satoh-Chin formalism [5]. The coherent frequencies are given by numeric solution of an eigenvalue problem. The threshold of instability is defined by the mode crossing, usually mode $m = 0$ and $m = -1$. The results of calculations are shown in Fig. 6. The threshold bunch current is below 1 mA for the last 3 machines, but the nominal bunch current is also low and all machines should be stable.

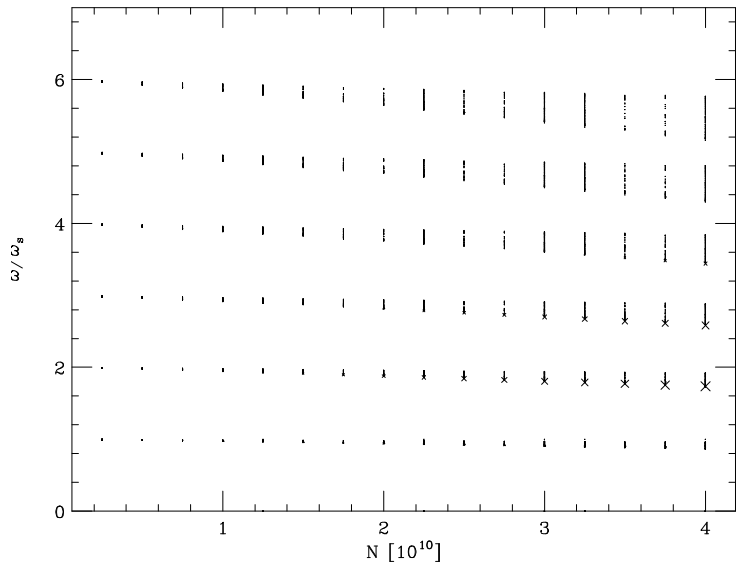

Figure 5: Result of the Oide's code for PPA. The growth rate of a mode is proportional to the size of the crosses in the plot. The code predicts the threshold of the microwave instability around $2.\,10^{10}$ particles per bunch

4 Conclusion

Overall, the conventional instabilities will have little impact on the ring performance provided the careful design of the ring minimizes the impedance below acceptable level indicated above. The only exception is the transverse CB instability. The longitudinal CB is less demanding. However, even the transverse CB instability would have threshold current above nominal provided the aperture in the wigglers is increased from 8 mm to 16 mm. The the microwave instability needs more studies.

Nevertheless, we should remember that the ILC DR is different from existing high-current machines at least in two respects: absence of the beam-beam tune spread stabilizing beams in colliders, and unusual strict requirements for low emittance. That may cause new problems such as bunch emittance dilution due to high-frequency wakes (BPMs, grooves), etc. Even if such a possibility exists, it probably universal for all machines and ought be addressed in the design of vacuum components rather than have effect on the choice of the machine design.

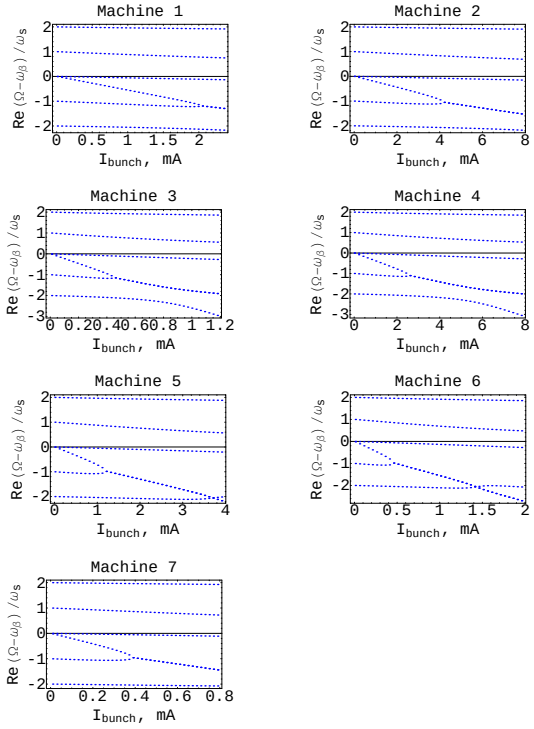

Figure 6: The head-tail instability. The threshold bunch current corresponds to the first crossing of the modes.

References

[1] A. Wolski, Lattices with Large Dynamic Aperture for ILC Damping Rings, Preprint LBNL-57045, LBNL (2005).

[2] TESLA Technical Design Report, Preprint DESY 2001-11, DESY (2001).

[3] KEK B-Factory Design Report, Report 95-7, KEK (1995).

[4] A.W. Chao, Physics of collective beam instabilities in high energy accelerators, J. Wiley and Sons, inc. 1993.

[5] K. Satoh and Y. Chin, Transverse mode coupling in a bunched beam, Nucl. Instr. and Methods, 207, (1983) 309-320